ELSEVIER

Journal of Molecular Catalysis A: Chemical 163 (2000) 105–116

JOURNAL OF MOLECULAR CATALYSIS A: CHEMICAL

www.elsevier.com/locate/molcata

Kinetic analysis of ammonia synthesis catalyzed by barium-promoted ruthenium supported on zeolite X

Brian C. McClaine, Thierry Becue, Carrie Lock, Robert J. Davis*

Department of Chemical Engineering, University of Virginia, Charlottesville, VA 22903-2442, USA

Received 3 February 2000; received in revised form 27 March 2000; accepted 6 June 2000

Abstract

The kinetics of ammonia synthesis from dinitrogen and dihydrogen were studied at 20.7 atm total pressure over a series of zeolite X supported Ru (∼2 wt.%) catalysts that were promoted by occluded barium. For comparison, two different Cs-promoted Ru/MgO catalysts were also included. In general, the reaction was first order in dinitrogen, about negative one order in dihydrogen, and weakly inhibited by ammonia. The average turnover frequencies of the Ba-promoted Ru/zeolite catalysts were within a factor of two of the highly active Cs-promoted Ru/MgO catalysts. The effect of Ba loading on an average turnover frequency and overall Ru metal utilization indicated an optimal content of 20 excess Ba cations per unit cell. A uniform surface model, assuming dinitrogen adsorption is the rate-determining step and both nitrogen and hydrogen atoms are present on the surface, reproduced well the measured kinetics over a wide range of temperatures and feed ratios. Results from fitting the kinetic parameters suggest that addition of basic promoters to supported Ru lowers the activation barrier for dinitrogen adsorption.

Keywords: Ruthenium ammonia; Synthesis of zeolite X barium; Promotion by reaction kinetics

1. Introduction

Synthesis of ammonia from dinitrogen and dihydrogen is among the most widely studied catalytic reactions, dating back to the beginning of the 20th century. Indeed, Michel Boudart refers to ammonia synthesis as the bellwether reaction in heterogeneous catalysis [1]. Typical commercial catalysts consist of either doubly promoted iron (Fe-Al_2O_3-K_2O) or triply promoted iron (Fe-Al_2O_3-CaO-K_2O). The Boudart laboratory has contributed significantly to the understanding of catalytic ammonia synthesis by studying magnesia-supported iron particles, in particular identifying the importance of particle size and surface reconstruction on the catalytic activity of supported iron [2,3]. The turnover frequency for ammonia synthesis, based on surface Fe atoms, increased by a factor of 35 as the particle size increased from 1 to 30 nm [2]. High pressure reactions conducted on iron single crystals showed unambiguously that the (1 1 1) surface orientation is the most active low index plane for ammonia synthesis [4]. It is generally accepted that C_7 sites (Fe atoms with 7 nearest neighbors) that are prevalent on the (1 1 1) surface of Fe are responsible for the high catalytic activity. The kinetics of ammonia synthesis are reasonably well described by a rate-determining step involving dinitrogen adsorption, followed by a sequence of elementary steps including dihydrogen adsorption, surface reactions, and desorption of ammonia [5]. Boudart and Djega–Mariadassou emphasize that the rate expression for ammonia syn-

* Corresponding author.
E-mail address: rjd4f@virginia.edu (R.J. Davis).

1381-1169/00/$ – see front matter
PII: S1381-1169(00)00403-9

thesis derived from uniform surface kinetics is almost experimentally indistinguishable from that obtained by assuming a nonuniform surface [5]. Thus, it is from the solid foundation of earlier work on the kinetics of ammonia synthesis over iron that we launch into the current study of novel supported catalysts.

Of all the active metals tested for ammonia synthesis, ruthenium is believed to be the basis of the next generation catalyst. The main advantages of the ruthenium catalysts are less inhibition by ammonia and greater tolerance of reaction poisons than iron-based catalysts [6]. Unlike iron-based catalysts, ruthenium-based catalysts are inhibited by dihydrogen. A promoted ruthenium catalyst supported on carbon has been developed for use in the Ocelot Ammonia Plant in British Columbia. In addition to lower capital costs, the energy consumption of the plant was reduced by 1 million BTU/t of ammonia produced compared to typical iron-based systems [7].

Due to the higher price of Ru compared to Fe, it is necessary to disperse Ru on a high surface area support in order to maximize the fraction of metal atoms participating in the catalytic reaction. In light of Boudart's earlier work with supported iron particles, the possible structure sensitivity of ammonia synthesis on supported Ru particles is of paramount importance. Aika et al. surveyed a wide variety of supported and unsupported Ru catalysts for ammonia synthesis at 588 K and 600 Torr total pressure and found the influence of promoters to be more important than the dispersion of Ru [8]. On the other hand, dinitrogen activation on a Ru single crystal was recently found to be totally dominated by the steps in the surface which act as low barrier channels to populate terraces [9]. Those results suggest that ammonia synthesis might be extremely sensitive to surface structure, with small particles being more active than large particles due to the larger relative fraction of low-coordinated edge sites on the former. Dooling et al. used density functional calculations to demonstrate that an open surface plane of Ru stabilizes dinitrogen in a precursor state that most likely leads to dissociation whereas a close-packed face of Ru could not [10]. It appears that small particles of supported Ru that expose low coordinated surface atoms might be excellent catalysts for ammonia synthesis, provided suitable promoters are found. To the best of our knowledge, the lower limit on Ru particle size that still exposes an active site has not yet been determined.

Zeolites are of particular interest as supports since the maximum size of occluded metal particles is limited to the size of the zeolite pores or cages. Also, the basicity of the zeolite is easily modified by ion exchange with Group IA and IIA cations, with the consensus being the promoter effectiveness for supported ruthenium catalysts increases with basicity.

Cisneros and Lunsford studied ammonia synthesis catalyzed by ruthenium supported on alkali-metal-exchanged zeolites X and Y [11]. The catalysts were found to be active at atmospheric pressure over the temperature range from 573 to 723 K, with ruthenium supported zeolite X being more effective. They found that the activity was strongly dependent on the zeolite cations, the turnover frequency increasing in the order Cs < Na < K for ion exchanged X zeolites. The turnover frequency was a factor of 25 less over Ru/CsX compared to Ru/KX at 350°C, presumably due to the relatively low level of Cs exchange in the sample.

We have previously synthesized nanometer-size Ru metal clusters inside the cages of KX zeolite and promoted the catalyst with occluded K and Ba compounds [12]. The promotional effect of Ba on Ru-catalyzed ammonia synthesis at 20.7 atm was superior to that of K, which is counter to the anticipated basicity of the occluded compounds. In the present work, we synthesized a new set of Ba-promoted Ru catalysts and obtained the kinetic parameters for a rate expression that was based on uniform surface kinetics.

2. Experimental methods

2.1. Catalyst preparation

Preparation of the ruthenium catalysts was based on a method described by Oukaci et al. [13]. Potassium X zeolite was obtained by ion exchanging NaX zeolite (Union Carbide, 632 $m^2\,g^{-1}$) three times with a 1 M KNO_3 aqueous solution for 24 h at room temperature. Incorporation of Ru (2.0 wt.%) was accomplished by ion exchange of the KX zeolite in an aqueous solution of $Ru(NH_3)_6Cl_3$. The Ru^{3+} exchanged compounds were then washed with deionized distilled water. The absence of chloride was confirmed by silver nitrate

tests of the filtrates. The Ru/KX samples were reduced before any further ion exchanges. A sample was first dehydrated by heating under vacuum at 0.5 K min^{-1} to 723 K and held at that temperature for 1 h. After cooling to room temperature under vacuum, the dehydrated sample was then heated in flowing H_2 (palladium diffused, 20 ml min^{-1} g^{-1}) at 1 K min^{-1} to 723 K and reduced at 723 K for an additional 2 h. The Ru/KX was then cooled under vacuum (final pressure less than 10^{-5} Torr) and placed in a humid atmosphere overnight. The re-hydrated Ru/KX was ion-exchanged three times at room temperature in a 1 M barium acetate solution, filtered and washed. Barium was added to the catalysts beyond ion-exchange capacity by successive impregnations of 1 M solutions of $Ba(OH)_2$. The catalysts are designated according to the number of Ba cations per unit cell of zeolite.

A Ru/CsMgO compound was also prepared as a reference material. Ruthenium (∼2 wt.%) was added to magnesia (Ube Industries, 42 m^2 g^{-1}) by impregnation of $Ru_3(CO)_{12}$ dissolved in THF. The sample underwent the same reduction procedure described above for the zeolite-supported ruthenium catalysts. After reduction, cesium was added as a promoter (∼1:1 Cs:Ru) by impregnation of aqueous cesium acetate. The acetate was decomposed by heating the sample in flowing N_2 (50 ml min^{-1} g^{-1}) at 1 K min^{-1} to 773 K.

All catalysts were pressed into pellets, crushed and sieved between 250 and 425 μm. A 1.0 g sample was prepared for the single pass, tubular reactor using quartz wool to hold the catalyst sample in place.

2.2. Adsorption of dihydrogen

Chemisorption of dihydrogen was performed on a Coulter Omnisorp 100CX instrument. Before chemisorption, a sample was first heated in vacuum at 2 K min^{-1} to 673 K, reduced in flowing dihydrogen for 30 min, and evacuated again at 673 K for 45 min (final pressure less than 10^{-6} mbar). The samples were cooled in vacuum to room temperature prior to chemisorption of dihydrogen. Dihydrogen (BOC Gases, 99.999%) was passed through an OMI-2 purifier before admission to the sample. The amounts of total and reversibly adsorbed hydrogen were determined by extrapolating the linear part of the adsorption isotherms to zero pressure. The amount of irreversibly adsorbed hydrogen was calculated from the difference between the adsorption and backsorption (reversible) isotherms. The turnover frequencies presented in this work are calculated by normalizing the average rate of ammonia production (determined at the reactor outlet) by the number of surface Ru atoms titrated by irreversibly adsorbed hydrogen atoms.

2.3. Ammonia synthesis reactor

The reactor used for evaluation of the various catalysts was a 5 cm^3 fixed bed, single pass, tubular reactor operating at 20.7 atm. The reactants consisted of dinitrogen (BOC Gases, 99.999%) and dihydrogen (BOC Gases, 99.999%). Helium (BOC Gases, 99.999) was sometimes used as a diluent. The gases were mixed in appropriate ratios and passed over a guard bed (MnO/SiO_2 and molecular sieves) to remove trace amounts of dioxygen and water prior to entering the reaction zone. Analysis of the reactor effluent was accomplished by gas chromatography utilizing a thermal conductivity detector (TCD).

The TCD response to ammonia was calibrated by allowing the ammonia synthesis reaction to reach equilibrium at 1.0 and 20.7 atm. The TCD peak areas from the equilibrated mixtures were then compared with ammonia partial pressures derived from either thermodynamic calculations or previously reported experimental results. The equilibrium constant at atmospheric pressure was calculated from the Gibbs free energy of formation, where ΔG is a function of temperature given by the Gibbs–Helmholtz equation. The heat of reaction was determined from the enthalpy polynomial coefficients for dihydrogen, dinitrogen and ammonia obtained by Christiansen and Kjaer [14]. The equilibrium pressure of ammonia at 20.7 atm was determined from the experimental results of Larson and Dodge [15]. Values of the equilibrium ammonia partial pressure at a variety of conditions were obtained and correlated with the corresponding TCD peak areas from our equilibrium reaction runs. The TCD response for ammonia in an equilibrated mixture (dashed line) at atmospheric pressure is shown in Fig. 1 for a variety of total flow rates.

2.4. Kinetic model

The kinetics of ammonia synthesis over ruthenium are considerably different than what has been reported

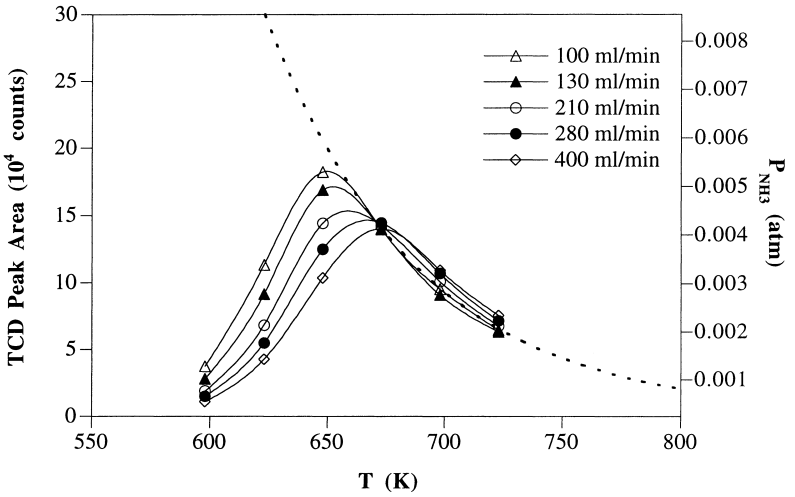

Fig. 1. GC response for ammonia over Ru/CsMgO (B) (1 atm, N_2:H_2 = 1:3). The thermodynamic equilibrium ammonia pressures were determined from the Gibbs–Helmholtz equation.

over iron catalysts. For example, the reaction order in dihydrogen is positive over iron but negative over ruthenium. In addition, the synthesis reaction is not as strongly inhibited by ammonia on Ru compared to Fe.

For ammonia synthesis on either Ru or Fe, the dissociative adsorption of dinitrogen is likely to be rate-determining since the bond energy (941 kJ mol^{-1}) of dinitrogen is the highest among diatomic molecules. Indeed, the forward rate of ammonia synthesis on Ru is first order in dinitrogen. A negative reaction order in dihydrogen suggests that adsorbed hydrogen atoms cover a large fraction of the Ru surface sites. Assuming dissociative adsorption of N_2 is the rate-determining step and both H and N atoms are present on the surface in kinetically significant amounts, the following sequence for the reaction is proposed to occur on Ru catalysts:

Step1 $N_2 + 2^* \rightleftharpoons 2N^*$

Step2 $H_2 + 2^* \rightleftharpoons 2H^*$

Step3 $N^* + 3H^* \rightleftharpoons NH_3 + 4^*$

where * represents an active site on a uniform surface. Steps 2 and 3 are considered to be quasi-equilibrated. Note that step 3 is not an elementary step but an overall reaction composed of catalytic hydrogenation steps and ammonia desorption. The net rate is expressed in terms of the rate-determining step

$$\text{rate} = k_1[N_2][^{**}] - k_{-1}[N^{**}N] \quad (1)$$

where [**] and [N**N] represent the number density of empty pairs and occupied pairs of adjacent surface sites, respectively [5]. Since [**] is proportional to $[^*]^2[L]^{-1}$ and [N**N] is proportional to $[N^*]^2[L]^{-1}$, where [L] is the number density of sites on the catalyst, the rate of step 1 can also be written as

$$\text{rate} = \frac{k_{1'}[N_2][^*]^2}{[L]} - \frac{k_{-1'}[N^*]^2}{[L]} \quad (1a)$$

The number density of sites is equal to the sum of the concentrations of unoccupied sites and sites covered by the most abundant reactive intermediates

$$[L] = [^*] + [H^*] + [N^*] \quad (2)$$

From the definitions of the equilibrium constants for steps 1–3 and the overall reaction

$$K_1 = \frac{k_{1'}}{k_{-1'}} \quad (3)$$

$$K_2 = \frac{[H^*]^2}{[^*]^2[H_2]} \quad (4)$$

$$K_3 = \frac{[NH_3][^*]^4}{[N^*][H^*]^3} \quad (5)$$

$$K_p = K_1^{1/2} K_2^{3/2} K_3 \quad (6)$$

the following rate expression for the reaction on a uniform surface is derived

$$\text{rate} = \frac{k_1'[L]\{[N_2] - [NH_3]/K_p^2[H_2]^3\}}{\{1 + K_2^{1/2}[H_2]^{1/2} + K_1^{1/2}[NH_3]^2/K_p[H_2]^{3/2}\}} \quad (7)$$

Differential conversion in the reactor was not assumed since most of the rate data were determined at outlet ammonia concentrations greater than 20% of the equilibrium concentration. The rate expression was evaluated throughout the reactor to properly account for inhibition of the reaction by ammonia.

Ertl et al. performed a microkinetic analysis of dinitrogen reactions on Ru/Al_2O_3, Ru/MgO and cesium-promoted Ru/MgO [16–19]. Results from the N_2 isotopic exchange reaction and temperature program adsorption/desorption experiments were used to derive the pre-exponential factors and activation energies for dissociative adsorption and associative desorption of dinitrogen. Since the pre-exponential factors for dinitrogen adsorption and desorption, k_{1O}' and k_{-1O}', were found to be nearly independent of promoter ($k_{1O}' = 56\,s^{-1}\,kPa^{-1}$ and $k_{-1O}' = 2.0 \times 10^{10}\,s^{-1}$), we used those values as fixed constants in our kinetic model. Likewise, the enthalpy of dinitrogen adsorption (E_{ads}–E_{des}) was also observed to be fairly independent of catalyst composition, and an average value of $\Delta H_{N_2} = -105\,kJ\,mol^{-1}$ was used in our kinetic model. Incorporating these three constants into our rate expression reduced the number of unknown kinetic parameters to three: the activation energy for dinitrogen adsorption (E_1), the pre-exponential factor of the dihydrogen adsorption equilibrium constant (K_{2O}) and the enthalpy of dihydrogen adsorption (ΔH_{H_2}). The number density of active sites [L] in our work is based on the amount of irreversibly chemisorbed hydrogen atoms. Since the site density used by Ertl et al. was derived from adsorption of dinitrogen, the basis of K_{2O} in our work is different by about a factor of 3. A minimization routine in MATLAB was then performed on the following objective function to determine the best fit kinetic parameters (where X is the conversion of dinitrogen and N the total number of data sets per catalyst):

$$SSQ = \sum_{i=1}^{N} (X_{calc} - X_{meas})^2 \quad (8)$$

3. Results

The chemical compositions of the catalysts determined from elemental analysis and results from dihydrogen chemisorption are found in Table 1. Samples prepared and tested by Becue et al. are labeled with (B) [12]. A completely new set of samples was prepared for this study to check for reproducibility of the promotional effects of barium. These new samples are denoted with (M). Catalyst compositions are expressed in terms of an ideal zeolite unit cell have

Table 1
Results from elemental analysis and H_2 chemisorption of the supported Ru catalysts

Catalyst	H/Ru_{total}	H/Ru_{irrev}	Support composition by unit cell
Ru/BaX-31 (B)[a]	0.94	0.46	$Ru_{3.8}Na_{2.1}K_{9.6}Ba_{31.4}H_{9.6}Al_{84.5}Si_{107.5}O_{384}$
Ru/BaX-35 (B)[a]	0.94	0.46	$Ru_{3.6}Na_{1.9}K_{8.6}Ba_{35.4}H_{3.4}Al_{84.7}Si_{107.3}O_{384}$
Ru/BaX-43 (B)[a]	1.10	0.56	$Ru_{3.4}Na_{1.7}K_{8.4}Ba_{43.1}Al_{85.0}Si_{107.0}O_{384}$
Ru/BaX-52 (B)[a]	1.49	0.72	$Ru_{3.4}Na_{4.2}K_{10.7}Ba_{52.3}Al_{87.6}Si_{104.4}O_{384}$
Ru/CsMgO (B)[a]	1.38	0.81	Cs loading 5.47 wt.%; Cs/Ru = 2.0
Ru/BaX-33 (M)[b]	0.78	0.38	$Ru_{3.4}Na_{1.3}K_{5.4}Ba_{32.8}H_{7.0}Al_{79.3}Si_{112.7}O_{384}$
Ru/BaX-41 (M)[b,c]	1.20	0.58	$Ru_{3.1}Na_{1.3}K_{5.4}Ba_{41.3}Al_{77.7}Si_{114.3}O_{384}$
Ru/BaX-51 (M)[b,c]	1.27	0.52	$Ru_{3.2}Na_{1.3}K_{5.4}Ba_{50.8}Al_{77.7}Si_{114.3}O_{384}$
Ru/BaX-65 (M)[b,c]	0.93	0.46	$Ru_{3.1}Na_{1.3}K_{5.4}Ba_{65.4}Al_{77.7}Si_{114.3}O_{384}$
Ru/CsMgO (M)[b]	1.50	0.95	Cs loading 1.62 wt.%; Cs/Ru = 1.0

[a] Samples prepared by Becue et al. [12].
[b] Samples prepared in this work.
[c] Sodium and potassium are nominal loadings.

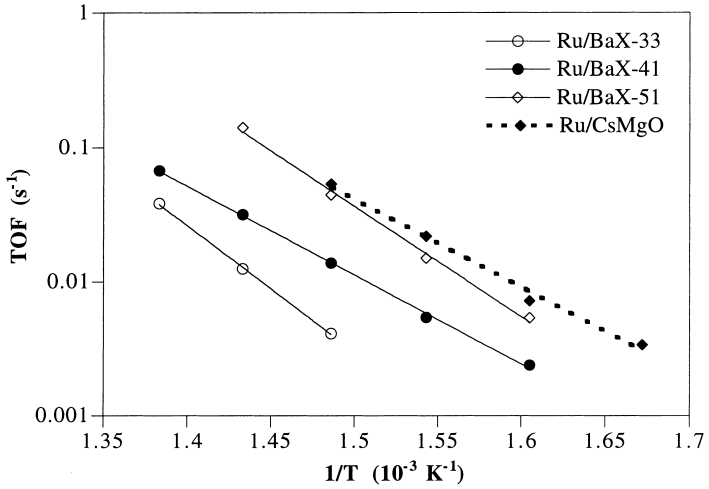

Fig. 2. Turnover frequencies for ammonia synthesis at 20.7 atm over 1.0 g Ru/BaX (M) with different loadings of excess barium, compared to Ru/CsMgO (M) (N_2:H_2 = 1:3, constant ammonia pressure of 0.001 atm).

384 oxygen atoms bridging tetrahedral Si and Al. In some cases, protons were added to the unit cell formula to satisfy charge neutrality. Barium was loaded onto the catalysts above the total ion-exchange capacity in order to deposit occluded basic promoters. The fraction of Ru exposed, determined by dihydrogen chemisorption, was high in all cases including the nonzeolite catalyst Ru/CsMgO. Thus, the differences in observed rates among the catalyst samples can be attributed mostly to the influence of promoters.

In general, the ammonia synthesis reaction on our supported Ru catalysts was approximately first-order in dinitrogen, minus one order in dihydrogen and slightly inhibited by ammonia (see Becue et al. [12] for typical reaction order plots). Arrhenius-type plots for representative catalysts are presented in Fig. 2. Turnover frequencies and apparent activation energies reported in Table 2 are calculated from results at both constant flow rate and constant ammonia pressure (using observed reaction orders in ammonia).

Table 2
Rates and apparent activation energies of ammonia synthesis over supported Ru Catalysts at 20.7 atm and stoichiometric feed

Catalyst	TOF c.f.[a] (10^{-4} s^{-1})	E_a[b] (kJ mol^{-1})	TOF c.p.[c] (10^{-4} s^{-1})	E_a c.p.[d] (kJ mol^{-1})
Ru/BaX-31 (B)	25.3	154	41.3	180
Ru/BaX-35 (B)	45.4	133	129	157
Ru/BaX-43 (B)	98.6	119	361	122
Ru/BaX-52 (B)	130	122	543	124
Ru/CsMgO (B)	292	123	890	148
Ru/BaX-33 (M)	20.8	113	54.3	160
Ru/BaX-41 (M)	86.1	113	138	126
Ru/BaX-51 (M)	138	123	445	157
Ru/BaX-65 (M)	95.3	103	542	152
Ru/CsMgO (M)	276	111	536	125

[a] Turnover frequency measured at constant flow rate (400 cm^3 min^{-1}) and 673 K.
[b] Calculated at constant flow rate.
[c] Turnover frequency calculated at constant ammonia partial pressure (P_{NH_3} = 0.001 atm).
[d] Calculated from turnover frequencies at constant ammonia pressure.

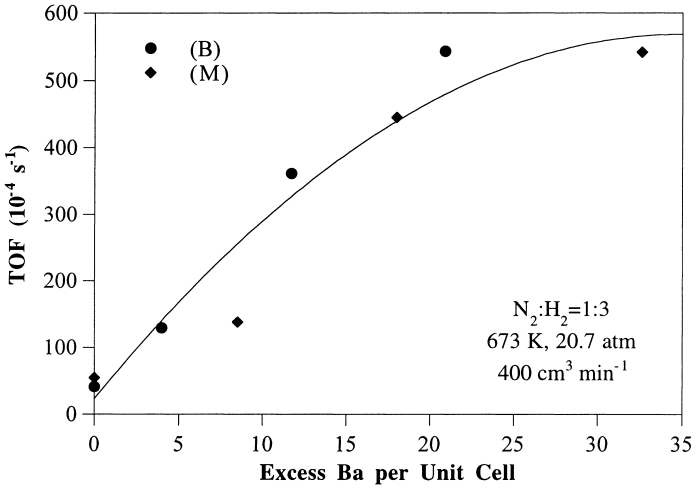

Fig. 3. Effect of excess barium on turnover frequency calculated at constant ammonia pressure (0.001 atm).

Clearly, addition of barium to the Ru-zeolites beyond ion-exchange capacity improved the TOF at constant ammonia pressure by an order of magnitude (Table 2, Fig. 3). The agreement between the two sets of catalyst samples (B) and (M) demonstrates the excellent reproducibility of the catalyst synthesis procedures as well as the trends with barium promotion. It appears that the TOF at constant ammonia pressure (Fig. 3) reaches a constant value after addition of about 20 excess Ba atoms per unit cell. Fig. 4 shows that increasing the amount of added barium eventually results in a decrease in the overall amount of ammonia produced for an equivalent amount of metal loaded in the reactor. Evidently, metal utilization decreases at very high Ba loadings, presumably due to pore blockage, loss of crystallinity, and/or excessive coverage of the Ru metal by Ba.

Results from the fitting procedure were used to derive the kinetic parameters presented in Table 3. The enthalpy of dihydrogen adsorption varied over the

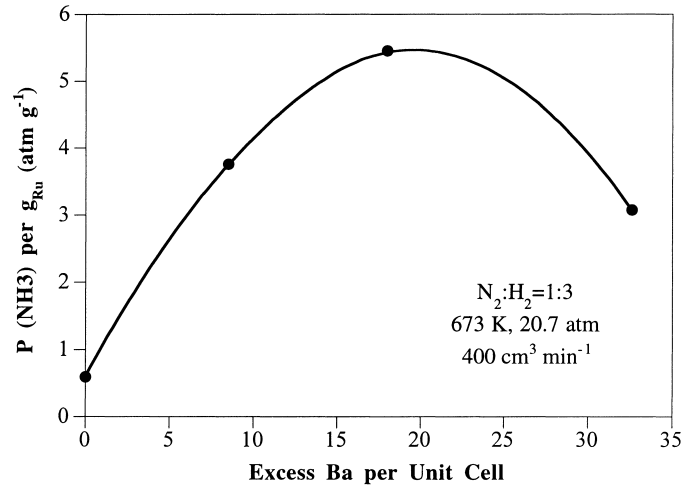

Fig. 4. Effect of excess barium on metal utilization for ammonia synthesis over Ru/BaX (M) samples. The vertical axis represents the ammonia pressure at the reactor outlet divided by the total Ru loading in the reactor for runs with similar catalyst charges.

Table 3
Fitted kinetic parameters for supported Ru catalysts

Catalyst	E_1 (kJ mol^{-1})	K_{2O} (atm^{-1})	$-\Delta H_{H_2}$ (kJ mol^{-1})
Ru/BaX-43 (B)	54.0	5.46×10^{-6}	72.6
Ru/BaX-52 (B)	54.3	5.75×10^{-4}	83.2
Ru/CsMgO (B)	41.1	2.08×10^{-5}	84.9
Ru/BaX-33 (M)	71.3	4.33×10^{-5}	65.0
Ru/BaX-41 (M)	55.0	5.92×10^{-5}	71.8
Ru/BaX-51 (M)	44.1	4.03×10^{-5}	82.8
Ru/CsMgO (M)	32.5	1.81×10^{-4}	81.8

fairly narrow range from 65 to 85 kJ mol^{-1}, whereas the activation energy for dinitrogen adsorption ranged from 32 to 71 kJ mol^{-1}, depending on catalyst sample. A comparison between the calculated and observed ammonia pressure at the reactor outlet over a wide range of conditions is shown in Fig. 5a and b for Ru/BaX-41 (M) and Ru/BaX-51 (M), respectively. The excellent agreement of the model to experimental results was also found for other catalysts, but those figures are not shown. The nearly inverse first order dependence of the rate on dihydrogen pressure at low conversion suggests that the middle term of the denominator of Eq. (7) can dominate the other terms. Thus, a strong correlation between k_1 and K_2 is expected at low ammonia pressures. Reliable determination of these two parameters requires fitting over a large range of conversions that approach equilibrium. Fig. 5(b) includes the degree to which E_1 and ΔH_{H_2} are coupled for the Ru/BaX-51 data set. The value for E_1 was varied (ΔE_1 both positive and negative) by 15 kJ mol^{-1} while maintaining the sum of E_1 and $(-\Delta H_{H_2})$ constant. The Ru/BaX-51 sample was the most active zeolite catalyst and exhibited the smallest influence of changing E_1. The clear differences in the model that was modified by $\pm$15 kJ mol^{-1} compared to experimental results show that E_1 and $(-\Delta H_{H_2})$ can be reasonably decoupled on all of the samples.

Fig. 6 [Ru/BaX-51 (M)] and 7 [Ru/CsMgO (M)], illustrate how well the optimized rate expression can be used to predict the outlet ammonia pressure over a wide range of feed mixtures, temperatures and conversions. The ammonia pressure decreased at the highest temperatures due to equilibrium limitations, which demonstrates that the model is thermodynamically consistent.

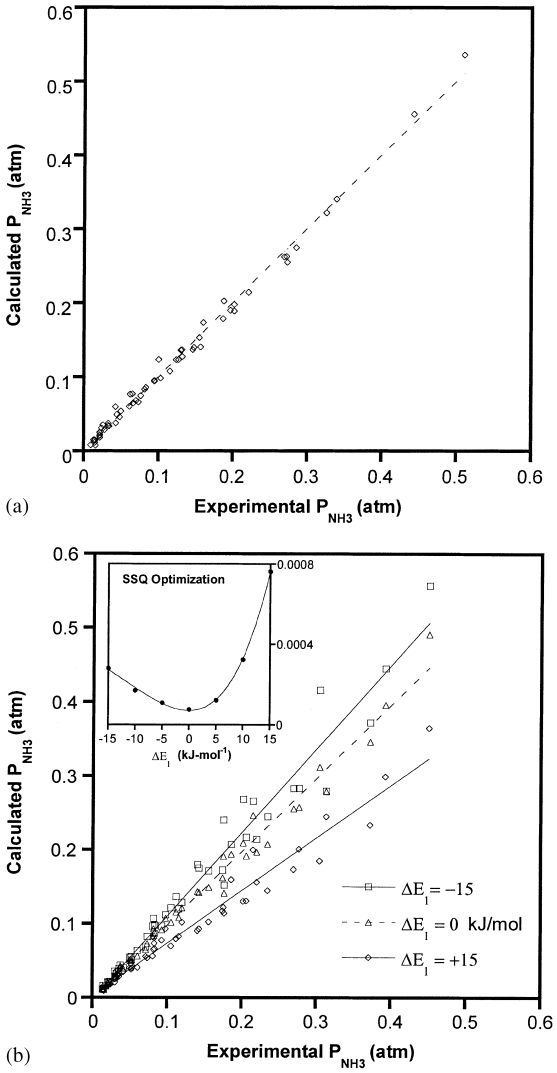

Fig. 5. (a) Comparison of calculated and experimental ammonia outlet pressures over Ru/BaX-41 (M). The data set spans a broad range of temperatures (648–723 K) and feed gas compositions (N_2:H_2 from 1:3 to 3:1). (b) Comparison of calculated and experimental ammonia outlet pressures over Ru/BaX-51, with $E_1 = E_1$ (minimum SSQ) $\pm$15 kJ mol^{-1} and $E_1 - \Delta H_{H_2} = 126.9$ kJ mol^{-1}.

The fractional coverages of adsorbed hydrogen and nitrogen atoms were determined from the calculated kinetic parameters. Fig. 8 shows the effect of N_2:H_2 ratio on the surface coverages on Ru/BaX-51 (M) at 673 K and constant ammonia pressure of 0.15 atm. A stoichiometric feed mixture resulted in a catalyst surface nearly covered with adsorbed H atoms. However,

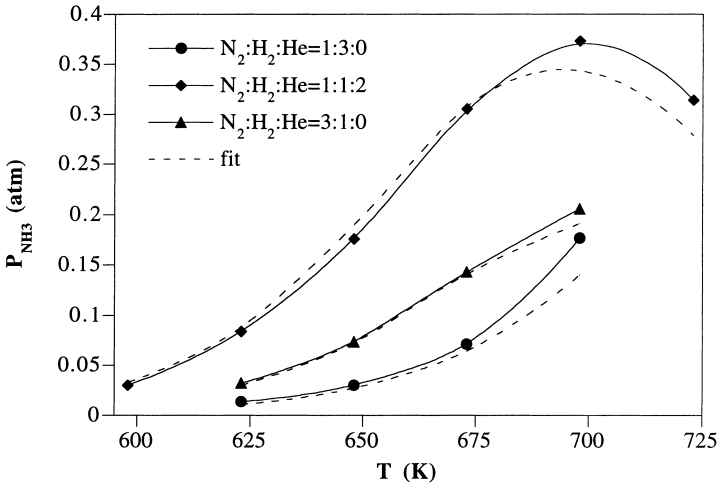

Fig. 6. Comparison of measured ammonia pressures determined at the outlet of a reactor containing Ru/BaX-51 (M) to the predicted values obtained from optimization of the rate expression. The total pressure in the reactor was 20.7 atm.

decreasing the relative pressure of dihydrogen substantially lowered the amount of adsorbed hydrogen atoms.

4. Discussion

The consistency of our ammonia synthesis rate measurements at elevated pressure on two completely different sets of catalysts, (sets (B) and (M), prepared years apart by different people) demonstrates that the substantial promotional effect of added Ba on zeolite-supported Ru is reproducible. The kinetic parameters for Ru/CsMgO, presented in Table 3, agree very well with those reported by Hinrichsen et al. ($\Delta H_{H_2} = -89.4\,\mathrm{kJ\,mol^{-1}}$, $K_{2O} = 2.4 \times 10^{-6}\,\mathrm{atm^{-1}}$ and E_1 of $33\,\mathrm{kJ\,mol^{-1}}$) for a similar Cs-promoted Ru/MgO catalyst [16]. Our results for

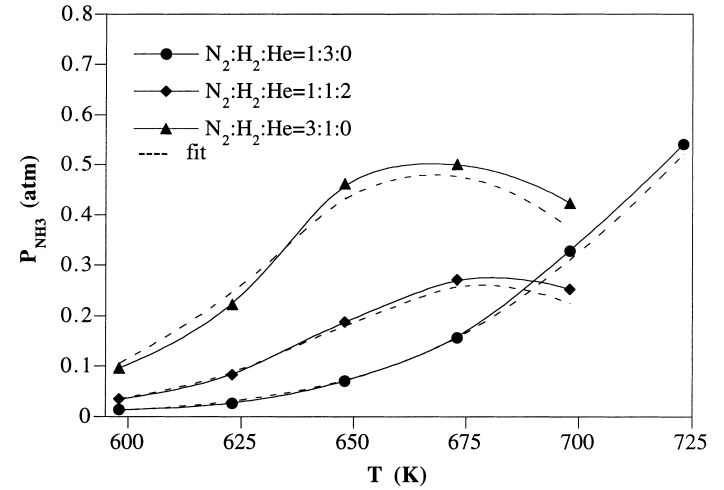

Fig. 7. Comparison of measured ammonia pressures determined at the outlet of a reactor containing Ru/CsMgO (M) to the predicted values obtained from optimization of the rate expression. The total pressure in the reactor was 20.7 atm.

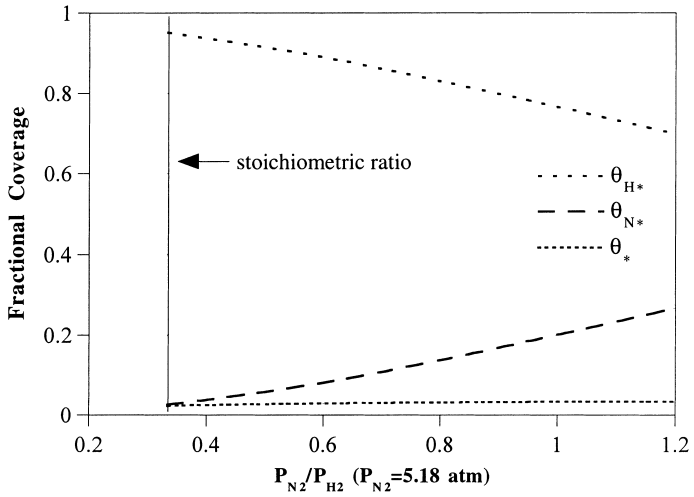

Fig. 8. Effect of N_2:H_2 feed ratio on the fractional coverage of hydrogen and nitrogen on Ru/BaX-51 (M) at 20.7 atm and 673 K. Dinitrogen partial pressure was held constant at 5.18 atm. Fractional coverages were calculated at constant ammonia pressure of 0.15 atm.

the Ba-promoted zeolite samples revealed a slightly higher barrier for dinitrogen dissociation, which suggests that the catalysts were not quite as effectively promoted as Ru/CsMgO.

At this time, the detailed mechanism of how the basic metals and oxides promote ammonia synthesis on Ru is not well understood. Aika et al. concluded that promotion is due to electron transfer from alkali metal promoters to ruthenium, noting the activity of ammonia synthesis increased with decreasing ionization potential of the added alkali metals [20].

More recently, Mortensen et al. studied the adsorption of dinitrogen on Ru(0 0 0 1) using DFT calculations and concluded that the effect of alkali metal promoters on Ru was mainly electrostatic in nature [21]. The promoter apparently lowers the barrier for dinitrogen dissociative adsorption without substantially affecting the stability of the reactant molecule and the nitrogen adatoms. This is an intriguing interpretation since it does not follow a Bronsted–Polanyi relationship, which correlates a change in activation barrier to a change in the stability of either the reactant or product. Clearly, the mechanism of Ru promotion by basic metals and metal oxides is an open question at this time.

For zeolite-supported Ru, we found that the activity did not scale solely with the anticipated basicity of the zeolite support [22]. Zeolites exchanged with alkaline earth ions were better supports than zeolites exchanged with alkali metal ions, even though the former are not considered as basic as the latter.

The Ru-zeolite catalysts studied in this work are complex materials composed of nanometer-size Ru metal clusters supported inside the supercages of zeolite X. In addition to charge balancing cations, barium hydroxide was occluded in the supercages, which may convert to barium oxide after thermal treatment. A surprising result reported earlier by our lab showed that Ru-zeolite catalysts containing occluded Ba were superior to those containing occluded K [12]. According to overall chemical compositions, the potassium-containing support materials should have been more basic, which usually translates into higher activities in ammonia synthesis. However, Bordawekar and Davis recently found that cesium oxide occluded in zeolite X has a much lower enthalpy for CO_2 adsorption than bulk cesium oxide, suggesting that the occluded oxide is a much weaker base [23]. The rather moderate basicity of alkali metal oxides occluded in zeolites may account for their modest promotional effect on ammonia synthesis on zeolite-supported Ru clusters. Additional studies are underway to characterize the chemical environment around occluded barium in the Ru-zeolites.

The kinetic parameters derived from our uniform surface kinetic model may shed some light on the role

of promoters in ammonia synthesis on Ru-zeolites. The assumption of constant enthalpy of dinitrogen adsorption used to fit the rate expression derived in this paper is consistent with the electrostatic mechanism of promotion described by Mortensen et al. [21]. Within the limitations of that assumption, we found that the activation barrier for N_2 dissociative adsorption was generally greater on the samples with lower activity. Even though the lowest activation barrier was associated with a highly active Ru/CsMgO sample, results from Ba-promoted Ru-zeolite catalysts are comparable. The appropriate support–promoter combination appears to lower the activation energy for dissociative adsorption of dinitrogen, which agrees with other theoretical and experimental studies [16–19,21].

It is interesting to note that the enthalpy for dihydrogen adsorption increases slightly on the more active samples (Table 3). A variety of studies have shown that the enthalpy of dihydrogen adsorption is approximately $100\,kJ\,mol^{-1}$ [24–28], which is greater than the values reported in Table 3. Since the parameters in Table 3 were derived from uniform surface kinetics, they are average values based on surface coverages achieved during ammonia synthesis, which can be quite high for adsorbed H atoms as illustrated in Fig. 8.

It is reasonable to question the use of uniform surface kinetics to describe the reaction rate on promoted Ru catalysts. Using steady state isotopic transient kinetic analysis (SSITKA), Nwalor et al. found that addition of potassium to Ru/SiO_2 increased by a factor of 16 the intrinsic turnover frequency of ammonia synthesis by creating an additional class of super active sites on the catalyst [29]. Promotion of Ru thus resulted in a more heterogeneous metal surface. Even though the new super active sites constituted only 20% of the total number of sites on the promoted catalyst, they accounted for 78% of the observed reaction rate, suggesting that the rate can be well approximated by the Langmuirian assumptions [29].

5. Conclusions

The promotional effect of occluded barium on the ammonia synthesis activity of zeolites-supported Ru catalysts has been reproduced and extended to higher barium loadings. The average turnover frequency for ammonia synthesis increased with Ba loading until a plateau was reached at about 20 excess Ba cations per zeolite unit cell. Beyond that loading, the overall effectiveness of Ru metal utilization decreased, suggesting that 20 excess Ba cations per unit cell is the optimal loading. A uniform surface kinetic model was derived assuming dinitrogen adsorption is the rate-determining step and both nitrogen and hydrogen adatoms were present on the surface in kinetically significant amounts. Results from parameter optimization indicated that the most active catalysts had the lowest activation barriers for dinitrogen adsorption, which is consistent with a previous microkinetic model reported by Ertl et al. [16]. The agreement between the model and experimental observations suggests that the assumption of uniform surface kinetics is reasonable for promoted Ru catalysts.

Acknowledgements

This work was supported by grants from the National Science Foundation (CTS-9729812) and the Academic Enhancement Program of the University of Virginia.

References

[1] M. Boudart, Top. Catal. 1 (1994) 405.
[2] J. Dumesic, H. Topsoe, S. Khammouma, M. Boudart, J. Catal. 37 (1975) 503.
[3] J. Dumesic, H. Topsoe, M. Boudart, J. Catal. 37 (1975) 513.
[4] N.D. Spencer, R.C. Schoonmaker, G.A. Somorjai, J. Catal. 74 (1982) 129.
[5] M. Boudart, G. Djega-Mariadassou, Kinetics of Heterogeneous Catalytic Reactions, Princeton University Press, Princeton, 1984.
[6] K. Aika, K. Tamaru, in: A. Nielsen (Ed.), Ammonia Catalysis and Manufacture, Berlin, 1 (1995) 104.
[7] Chementator, Chem. Eng. 3 (1993) 19.
[8] K. Aika, A. Ohya, A. Ozaki, Y. Inoue, I. Yasumori, J. Catal. 92 (1985) 305.
[9] S. Dahl, A. Logadottir, R. Egeberg, J. Larsen, I. Chorkendorff, E. Tornqvist, J. Norskov, Phys. Rev. Lett. 83 (1999) 1814.
[10] D. Dooling, R. Nielson, L. Broadbelt, Chem. Eng. Sci. 54 (1999) 3399.
[11] M.D. Cisneros, J.H. Lunsford, J. Catal. 141 (1993) 191.
[12] T. Becue, R.J. Davis, J.M. Garces, J. Catal. 179 (1998) 129.
[13] R. Oukaci, A. Sayari, J.G. Goodwin Jr., J. Catal. 106 (1987) 318.

[14] L.J. Christiansen, J. Kjaer (Eds.), Enthalpy Tables of Ideal Gases, Haldor Topsoe A/S, Copenhagen, 1982.
[15] A.T. Larson, R.L. Dodge, J. Am. Chem. Soc. 45 (1923) 2918.
[16] O. Hinrichsen, F. Rosowski, M. Muhler, G. Ertl, Chem. Eng. Sci. 51 (1996) 1683.
[17] O. Hinrichsen, F. Rosowski, A. Hornung, M. Muhler, G. Ertl, J. Catal. 165 (1997) 33.
[18] M. Muhler, F. Rosowski, O. Hinrichsen, A. Hornung, G. Ertl, Stud. Surf. Sci. Catal. 101 (1996) 317.
[19] F. Rosowski, O. Hinrichsen, M. Muhler, G. Ertl, Catal. Lett. 36 (1996) 229.
[20] K. Aika, H. Hori, A. Ozaki, J. Catal. 27 (1972) 424.
[21] J.J. Mortensen, B. Hammer, J.K. Norskov, Phys. Rev. Lett. 80 (1998) 4333.
[22] C.T. Fishel, R.J. Davis, J.M. Garces, J. Catal. 163 (1996) 148.
[23] S.V. Bordawekar, R.J. Davis, J. Catal. 189 (2000) 79.
[24] B. Fastrup, Catal. Lett. 48 (1997) 111.
[25] L. Danielson, M. Dresser, E. Donaldson, J. Dickinson, Surf. Sci. 71 (1978) 599.
[26] W. Tsai, W.H. Weinberg, J. Phys. Chem. 91 (1987) 5302.
[27] R. Narayan, N. Savargaonkar, M. Pruski, T. King, Stud. Surf. Sci. Catal. 101 (1996) 921.
[28] I. Toyoshima, G. Somorjai, Catal. Rev.-Sci. Eng. 19 (1979) 105.
[29] J.U. Nwalor, J.G.G. Jr., Top. Catal. 1 (1994) 285.